RESEARCH ARTICLE

WILEY

Batagay megaslump: A review of the permafrost deposits, Quaternary environmental history, and recent development

Julian Murton[1] | Thomas Opel[2] | Sebastian Wetterich[2,3] | Kseniia Ashastina[4] | Grigoriy Savvinov[5] | Petr Danilov[5] | Vasily Boeskorov[5]

[1]Permafrost Laboratory, Department of Geography, University of Sussex, Brighton, UK

[2]Alfred Wegener Institute Helmholtz Centre for Polar and Marine Research, Potsdam, Germany

[3]Current address: Technische Universität Dresden, Institute of Geography, Dresden, Germany

[4]Max Planck Institute for Geoanthropology, Jena, Germany

[5]Science Research Institute of Applied Ecology of the North, North-East Federal University, Yakutsk, Russia

Correspondence

Julian Murton, Permafrost Laboratory, Department of Geography, University of Sussex, Brighton BN1 9QJ, UK.
Email: j.b.murton@sussex.ac.uk

Abstract

The Batagay megaslump, in the Yana Uplands of northern Yakutia, Russia, is the largest known retrogressive thaw slump in the world. The slump exposes a remarkable sequence of Ice Age permafrost deposits that record the interaction of colluvial, eolian and periglacial processes on a hillslope episodically forested during the last 650 ka or more in response to climate variability on glacial–interglacial timescales. Numerous bones, teeth, and occasional carcasses of Pleistocene and Holocene mammals have been recovered from the permafrost. The megaslump developed over the course of several decades in three stages: (1) gullying, (2) thaw slumping, and (3) megaslumping. After disturbance to the taiga vegetation cover in the 1940s–1960s, a hillslope gully formed by the early 1960s. The gully initiated thaw slumping along its central part during the 1980s, with the slump enlarging to megaslump (>20 ha) proportions during the 1990s. By 2019, the area of the slump had reached about 80 ha and its headwall above the slump floor was up to about 55 m high. The main geomorphic processes of slump growth are headwall ablation and thermal erosion, producing a distinctive terrain of icy badlands on the slump floor. Though much of the megaslump is rapidly growing at present, it will probably stabilize eventually as an irregular terrain characterized by sandy ridges and sand-filled elongate depressions formed by degradation of the badlands. Comparison of the Batagay megaslump with megaslumps from northwest Canada reveals several similarities and differences in terms of their geomorphology, permafrost deposits, and Quaternary history.

KEYWORDS
gullies, permafrost, retrogressive thaw slumping, thermal erosion, thermokarst

1 | INTRODUCTION

The Batagay megaslump (Figure 1) is a huge thermokarst landform initiated by thermal erosion and enlarged by thaw slumping. The megaslump is categorized as a retrogressive thaw slump, a type of slope failure characterized by melt of exposed ground ice and slumping of thawed sediment.[1] Thaw slumping commonly starts where ice-rich permafrost is exposed by erosion, active-layer detachment, gullying, forest fires, construction, or mining.[2] Where the exposure reveals massive ice, large ice wedges, or abundant segregated ice, slumping may quickly enlarge the exposure to produce a steep or vertical headwall that overlooks a low-gradient floor covered by slumped soil.
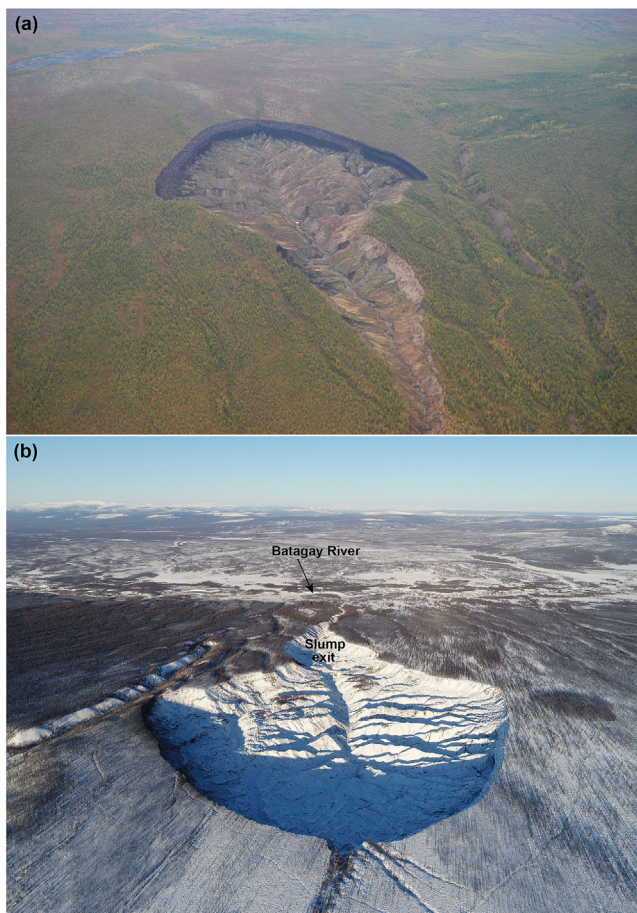
FIGURE 1 Aerial photographs of the Batagay megaslump. (a) Looking upslope (southwestward), summer 2015. (b) Looking downslope (northeastward) towards the Batagay River, March 22, 2019. Photographs © A. Gabyshev (a) and A. Kizyakov (b)

Slumps whose surface area exceeds 20 ha have been distinguished as *megaslumps*.[3] The Batagay slump exceeds 80 ha in area and is the largest known megaslump in the world. It is growing rapidly and exposes a remarkable sequence of Ice Age permafrost deposits that extends back to the Middle Pleistocene,[4] attracting international media interest as the so-called Batagaika crater (e.g.,[5,6]). Based on the available literature, the present article reviews the regional setting and outlines the permafrost deposits and their record of late Quaternary environmental history. It focuses on the geomorphological description of the landforms and processes associated with the slump, and on the chronology of slump development.

2 | REGIONAL SETTING

The Batagay megaslump is in the Yana Uplands of northern Yakutia, Russia (Figure 2). The uplands lie to the east of the Orulgan Range (part of the Verkhoyansk Range) and to the west of the Chersky Range. They reach elevations of 1,000–2,000 m above sea level (asl) and form the southern region of the Yana River basin.

Tectonically, the Batagay region is within the Verkhoyansk fold-and-thrust belt, which is composed of Carboniferous to Jurassic clastic sedimentary rocks deposited on the eastern passive continental margin of the Siberian Craton.[8] The rocks in the Batagay–Verkhoyansk area are mostly Triassic and Jurassic in age.[9] Rejuvenation of Late Cretaceous thrust systems contributed to the modern mountain relief of the Verkhoyansk fold belt. Several geological faults occur near Batagay, and earthquakes of up to magnitude 4–5 are recorded, as this is part of the Verkhoyansk earthquake region.

Climatically, the Verkhoyansk region has been considered the "Cold Pole" of the Northern Hemisphere because recorded winter air temperature can drop to nearly −68°C.[10] The climate is strongly continental. At Batagay, mean winter (December–February) air temperature over the period 1988–2017 was −40.0°C, mean summer (June–August) air temperature was 13.7°C, and mean annual air temperature (MAAT) was −12.4°C. Mean annual precipitation (MAP) was 203 mm, and mean summer precipitation was 106 mm. Since the mid-20th century, MAAT at Batagay has increased by about 2.4°C, summer mean air temperature has increased by about 1.6°C, MAP has increased by about 52 mm, and summer mean precipitation has increased by about 24 mm (Figure 3). Substantial variations in air temperature and precipitation from year to year, however, are shown by the low values of the associated coefficients of determination (R^2). The prevailing wind is from the southwest in January and from the north or northeast in July.

The vegetation near Batagay is dominated by open woodlands formed mainly of Dahurian larch (*Larix gmelinii*) with birch (*Betula nana* subsp. *exilis or B. divaricata*) undergrowth and a lichen–green moss ground cover. Dahurian larch averages 12–14 m in height and 10–14 cm in diameter. Birch (*B. pendula*) occurs in some burnt areas. Higher upland areas are characterized by thickets of dwarf stone pine (*Pinus pumila*), mountain tundra, or stony debris. The most common soil types beneath the open woodlands of larch are permafrost podburs. Underdeveloped stony soils characterize rubbly mountain areas, and peaty and humus–gley soils are found in the bottoms of small river valleys. Terraced floodplains of the Yana and Batagay rivers contain underdeveloped sandy soils and alluvial permafrost soils.

Permafrost in the Yana River valley is continuous, with mean annual ground temperatures at the top of permafrost of −8.0 to −5.5°C. The active layer is 0.2–0.4 m thick beneath forest and moss cover, and 0.4–1.2 m beneath open sites.[11]

The Yana Uplands have remained free of glacier ice for at least the last 50,000 years (citations in Murton et al. 2017[12]) and belonged to the unglaciated subcontinent of Beringia. Beringia was characterized by extensive silt, sand, and ice deposits frozen in permafrost beneath the land surface and covered by a mosaic of steppe and tundra plants that fed a rich animal fauna—including woolly mammoth, bison, and horse.[13] Dust storms sweeping across Beringia deposited huge amounts of silt and sand, burying the remains of many plants and some animals, which became frozen and preserved in the permafrost.[14,15] Beringia included not only lowlands[16] but some interior uplands—such as those of the Yana—distant from the moderating effects of coastal climates throughout the Quaternary and therefore

FIGURE 2 Map showing the topographic setting of the Batagay megaslump within the Yana River basin, northern Yakutia. Glacial limits during the last (Sartan) glaciation, according to Glushkova,[7] are indicated. Red dashed box shows the location of Figure 4
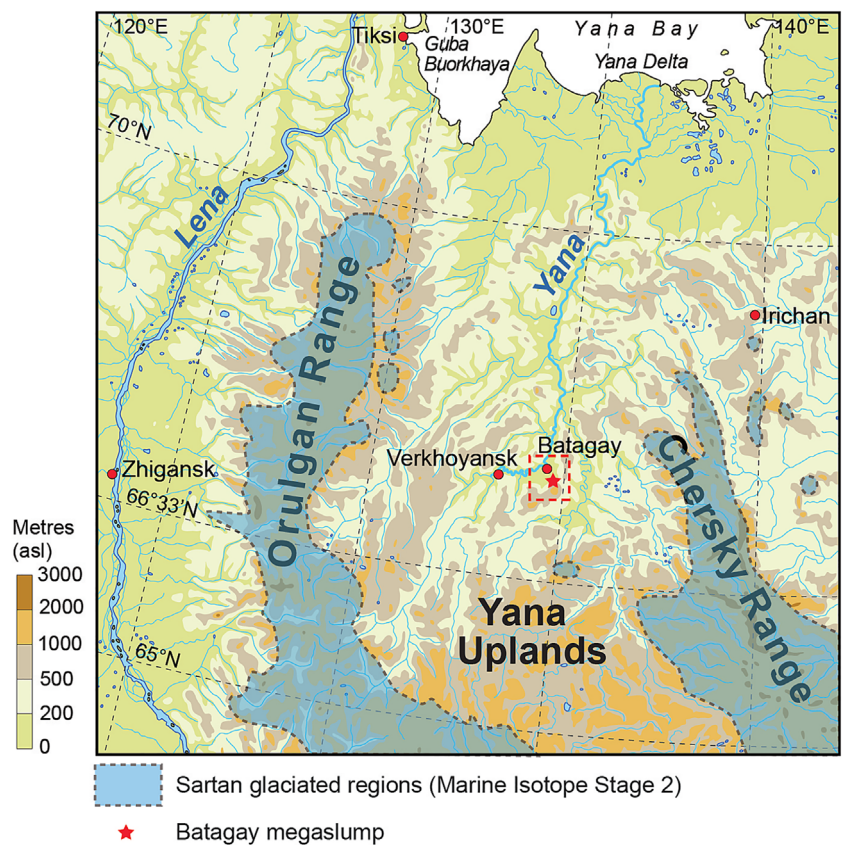

persistently continental (i.e., large annual temperature range, little precipitation, and relatively warm growing season). Such climatic persistence allowed meadow steppe vegetation—which formed the primary vegetation of the Yana Uplands during cold stages and a significant constituent of the plant cover during full warm-stage conditions—to grow there in varying proportions at least from about 190 to 15 ka.[17] Likewise, larch also persisted during this time, forming the dominant species in open coniferous woodland, similar to modern larch taiga during the last interglacial and surviving in stands during cold stages. The enduring meadow steppe vegetation in the Yana Uplands potentially provided pasture for large herbivores during both glacial and interglacial conditions. As a result, this region was a suitable refugium for organisms of the Pleistocene mammoth steppe.

3 | SITE DESCRIPTION

The Batagay megaslump (67°34′49.8″N, 134°46′19.3″E) is located 10 km southeast of the town of Batagay, in the Verkhoyansk region of northern Yakutia (Figure 4). The slump is on a northeast-facing hillslope about 1.5 km downslope of a col between Mount Kirgilyakh and Mount Khatyngnakh. The elevation of the ground surface on the uphill side of the site is about 290 m asl. The hillslope has a gradient of about 3° and is dissected by gullies that lead down into the floodplain of the Batagay River at about 150–160 m asl, a right-bank tributary of the Yana River.

The megaslump is shaped like a giant tadpole aligned southwest to northeast down the hillslope (Figures 1 and 5). A hillslope gully leads downslope into the center of the slump head, where it is truncated by the slump headwall. The orientation of the hillslope gully aligns with a primary gully that runs down the center of the slump floor. The exit of the slump tapers downslope towards the Batagay River. In 2019, the slump measured about 1.8 km long and had a maximum width of 0.89 km (Figure 5). The slump headwall is about 55 m high (Kizyakov et al., 2023[18]; Figure 6).

The bedrock at the megaslump is mainly slate, assigned to the Kedrovinsk Suite of Late Triassic (Norian) age.[19] The precursor rocks were aleurolites (siltstones) and argillites, which have undergone low-grade metamorphism into slate. The slate is dark gray and crops out intermittently in meltwater channels in the center of the slump floor and is exposed on the col crest about 2 km to the southwest. Quartz veins penetrate the slate, and tin has been extracted from cassiterite near Mount Kirgilyakh. On the hillslopes of Mount Khatyngnakh, the slate is intruded by dykes of diorite porphyry and dolerite of the Derbekin Complex (small diorite–dolerite intrusions) of Late Jurassic age. About 15 km south–southeast of the megaslump, granite crops out, marking the first phase of the Kolymsk Granite Complex, which intruded the Upper Triassic sedimentary rocks of the region during the Early Cretaceous. At this time, rhyolite dykes of the Kirgilyakh Complex (small granite–rhyolite intrusions) were emplaced into the country rock on Mount Kirgilyakh.
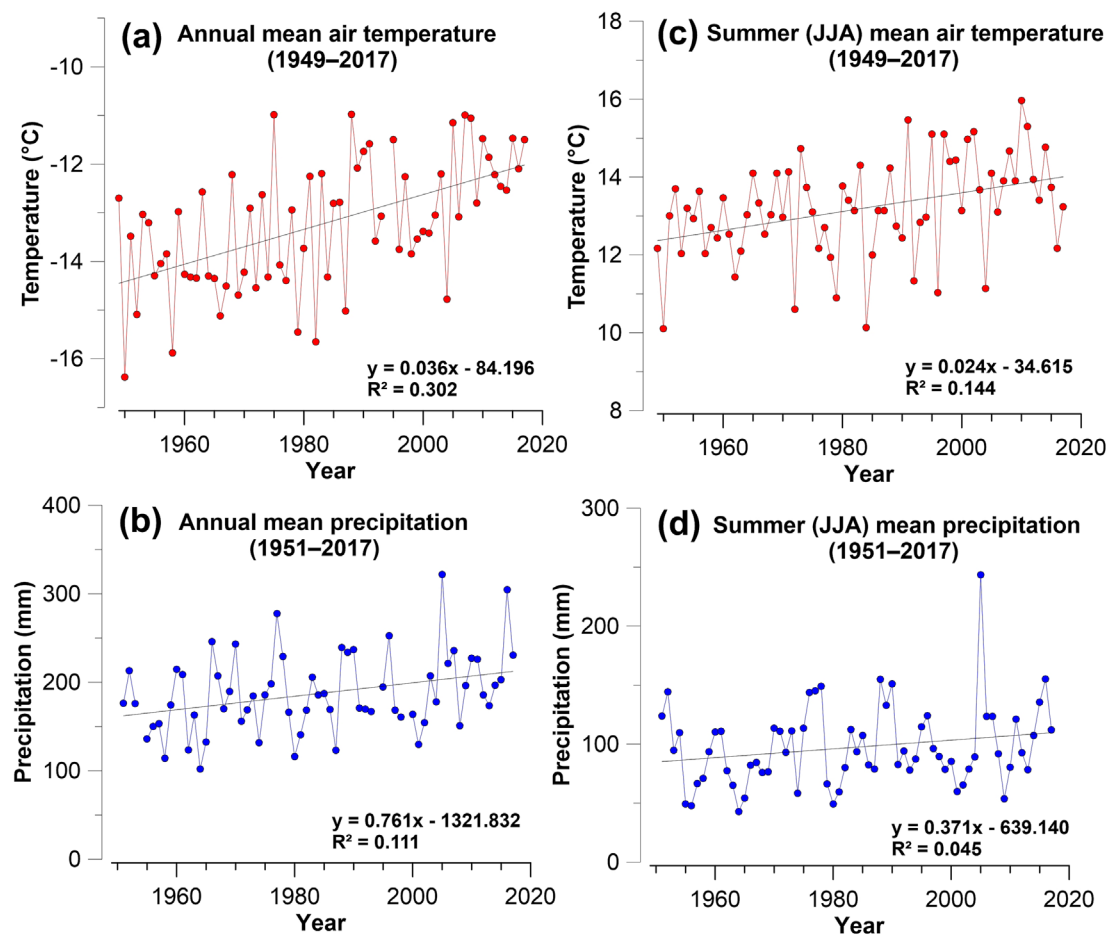
FIGURE 3 Climatic parameters at Batagay since the mid-20th century. (a) Annual mean air temperature, (b) annual mean precipitation, (c) summer (June–August) mean air temperature, and (d) summer (June–August) mean precipitation. Source of data: Yakutsk Department of the Federal Service for Hydrometeorology and Environmental Monitoring (Roshydromet)

The unconsolidated deposits mapped at and within several kilometers of the megaslump are dominantly sandy.[19] The upland (above about 200 m asl) to the northeast of the Batagay River valley is underlain by sand of the Tabalakh Suite (about 95 m thick), attributed to lacustrine and alluvial deposition during the Pliocene. In the Batagay River valley itself, sand, gravel, and loam (several meters to a few tens of meters thick) have been assigned to the first, second, and third terraces above the floodplain. The sand and gravel are attributed to deposition by alluvial and solifluction processes during the Pleistocene.

## 4 | PERMAFROST DEPOSITS AND QUATERNARY ENVIRONMENTAL CHANGE

4.1 | Cryostratigraphy and chronology

In outline, seven cryostratigraphic units have been identified from permafrost exposed in the slump headwall and floor (Table 1; Figure 6). A diamicton containing abundant clasts of slate overlies slate bedrock. The overlying lower ice complex contains woody material—including in situ tree stumps as well as woody debris related to erosional features within the ice complex—and ice wedges at least 2–3 m high and 1 m wide truncated along their tops by a thaw unconformity. There are also traces of an erosional surface overlain by gravelly deposits along the top of this unit. Above the lower ice complex, a lower sand unit of pore-ice-cemented fine sand contains tall, narrow syngenetic ice wedges and composite wedges up to 0.5 m wide. In places, prominent lenses of woody debris up to about 3 m thick sharply overlie the lower sand unit below a prominent disconformity (erosional surface). The woody debris is overlain by a few meters of sand at the base of an upper ice complex dominated by large syngenetic ice wedges up to a few meters wide and at least several meters high set within silty and sandy deposits. The upper ice complex plunges downslope beneath and partly grades into the upper sand unit (similar to the lower one), which is best exposed near the slump exit. Capping the sequence is a near-surface layer of brown sand and modern soil.

Several dating methods have been applied and combined to establish the chronology of the Batagay ancient permafrost, including optically stimulated luminescence (OSL) dating of quartz, infrared-stimulated (IRSL) and post-infrared infrared-stimulated luminescence

FIGURE 4 Topographic map of the Batagay region, showing the location of the megaslump on a NE-facing hillslope. Contours at 20-m intervals, grid spacing at 4 km
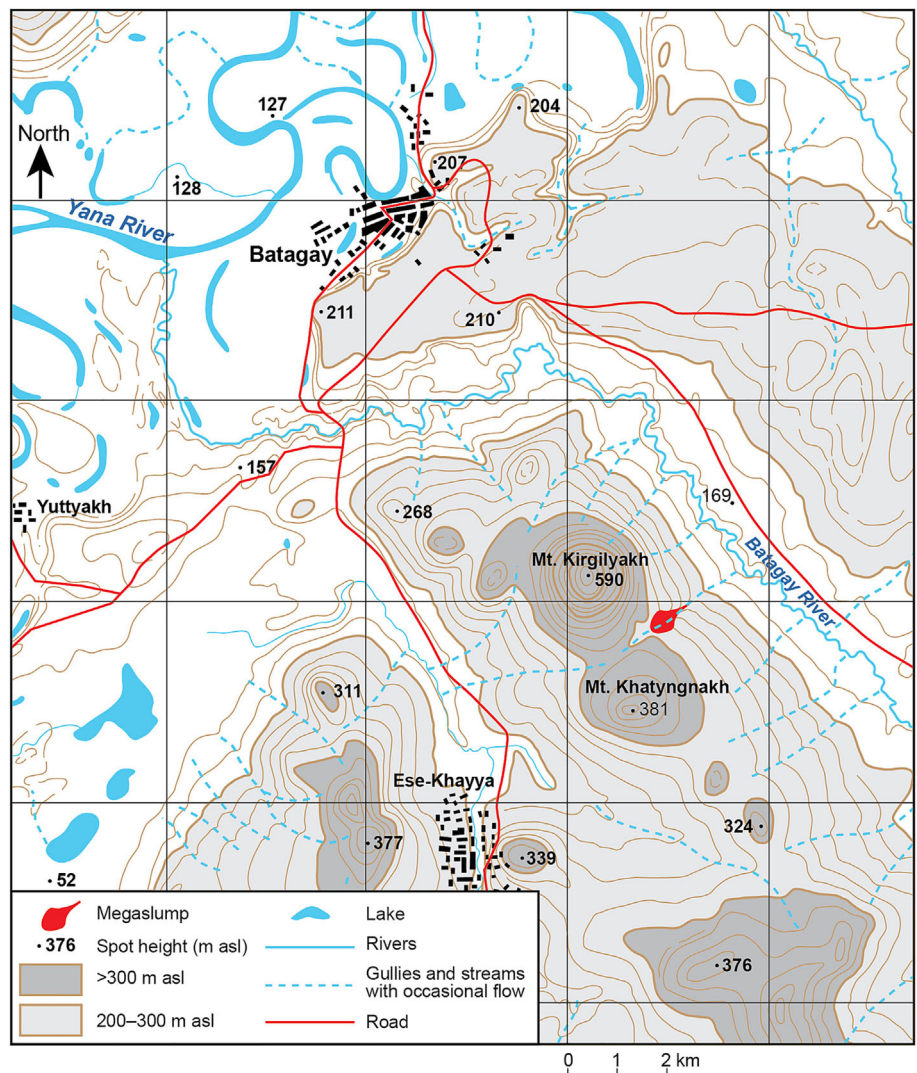
(pIR-IRSL) dating of feldspar, accelerator mass spectrometry-based [36]Cl/Cl dating of wedge ice and radiocarbon dating of organic material ([4] and references therein). These dating results for the ancient permafrost exposed in the Batagay thaw slump (Table 1) highlight its potential as a paleoenvironmental archive reaching back to at least the early Middle Pleistocene.

4.2 | Ground ice

The permafrost exposed in the Batagay thaw slump is very ice-rich, which promotes its high vulnerability to thaw. Kizyakov et al.[18] calculated volumetric ice contents in the deposits from the western headwall, including both the intrasedimental and the wedge-ice content per unit. The intrasedimental ice content of all considered cryostratigraphic units is quite comparable, varying between $47 \pm 7\%$ for the lower sand unit and $56 \pm 11\%$ for the upper ice complex. The other two main cryostratigraphic units show values in between, with $53 \pm 8\%$ for the lower ice complex and $51 \pm 10\%$ for the upper sand unit. The cryostructures of the frozen deposits that constitute the

intrasedimental ice content are described as massive (not visible), reticulate, lenticular, and layered in the upper and the lower ice complex units, and predominantly massive and lenticular in the upper and the lower sand units.[18]

The wedge-ice volume (WIV) of the cryostratigraphic units shows distinct differences and largely defines the overall ice content per unit.[18] The WIV of the upper ice complex is highest, reaching 70% and resulting in up to 87% total volumetric ice content, whereas the WIV of 56% in the lower ice complex results in 79% total ice content. Both sand units show much lower values of WIV, with only about 8% in the upper sand and up to 13% in the lower sand unit, resulting in 55 and 54% total ice content, respectively. The wedge ice of both sand units occurs as narrow (chimneylike) ice wedges or composite wedges, penetrating their entire respective horizons, but only up to 0.5 m wide. Truncated ice wedges of the lower ice complex are about 1.2–3.5 m tall and about 0.6–1.0 m wide,[18] and ice wedges of the upper ice complex penetrate the entire horizon of up to about 25 m thickness and reach up to a few meters in width.

Ice wedges of the lower and the upper ice complex units and the upper sand as well as composite wedges of the upper sand have been
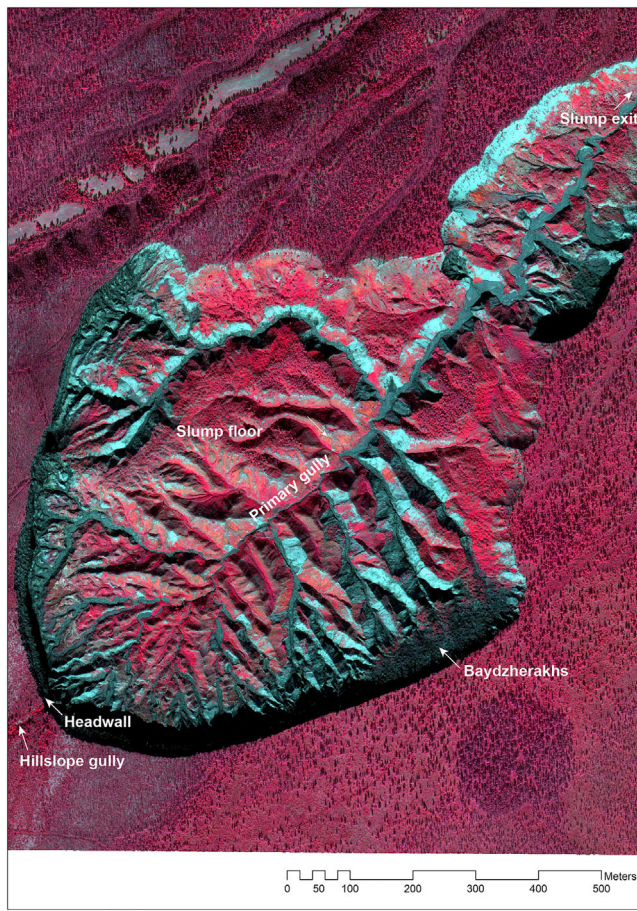
FIGURE 5 Satellite image (from WorldView-2) of the Batagay megaslump, August 15, 2016. The image has been pansharpened (fusion of spectral resolution of eight bands with 2-m resolution and panchromatic b/w band with spatial resolution of 0.5 m) and orthorectified to 0.5-m resolution (i.e., terrain corrected using a digital elevation model constructed from along-track WorldView stereo imagery of the same date). Band combination: false color infrared, red: near-infrared channel (860–1040 nm), green: red channel (630–690 nm), blue: green channel (510–580 nm). Red areas indicate vegetation, and blue areas indicate bare ground. Image courtesy of Frank Günther

analyzed for their stable water isotope composition ($\delta^{18}O$, δD, deuterium excess [d-excess]) to deduce past winter climate conditions.[21,24,25] Although the woody layer and the Holocene cover do not contain ice wedges or composite wedges, the composite wedges of the lower sand have not yet been studied. The mean $\delta^{18}O$ and d-excess values per ice wedge or composite wedge are summarized in Figure 7. The ice wedges of the upper ice complex show the most depleted $\delta^{18}O$ values and cluster around −35‰, suggesting that Marine Isotope Stages (MIS) 4–3 were characterized by the lowest winter temperatures preserved in Batagay ice wedges. These ice wedge $\delta^{18}O$ values are exceptional on a larger spatial scale (i.e., in east Siberia), and reflect the extreme continentality of the Batagay region.[21,24,25] The high d-excess values between 8 and 11‰ are also a specific feature of the Batagay ice wedges and indicate different

moisture sources and/or pathways compared to coastal ice wedge sites of the same age.[21] The ice wedges of the lower ice complex (MIS 16 or older) exhibit less depleted $\delta^{18}O$ values around −33‰, indicating less cold winters during formation. However, these values are close to those of intrasedimental ice sourced from summer to annual precipitation. This might point to postdepositional alteration of the original isotope signatures.[21] The ice wedges and composite wedges of the upper sand show less depleted $\delta^{18}O$ values between −33 and −30‰ and thus the largest variability and distinctly higher d-excess values. However, due to the small number of samples, the data are less conclusive for paleoclimatic interpretation of the MIS 3–2 deposits.

4.3 | Vertebrate remains

Numerous bones and some frozen carcasses of vertebrate fauna have been recovered from the site. The remains of *Dicrostonyx* spp. (collared lemming) provided a nonfinite ^{14}C age of >50,299 ^{14}C yr BP.[26] Using the "molecular clock" to estimate the age of this specimen yielded ∼333 ka BP (95% highest posterior density: 451–220 ka BP; Lord et al. 2022[27]), though the stratigraphic position of the specimen is not known. The recovered bones include the humerus of a cave lion (*Panthera spelaea*), the skull of a Pleistocene wolf (*Canis lupus*), and plenty of bones, teeth, and tusks of woolly mammoth (*Mammuthus primigenius*, the dominant species), Pleistocene bison (*Bison priscus*), and Pleistocene horse (*Equus lenensis*).[28] The majority of the remains were found in the central part of the slump floor on the ground surface, mainly beside small streams, though quite a lot of bones of mammoth, horse, and bison have been found directly beneath the headwall, probably fallen from the upper ice complex and upper sand unit. In general, the site has a typical "mammoth fauna," at least from the MIS 3 interstadial period of the Late Pleistocene. Two Holocene carcasses, of *E. lenensis* and juvenile *B. priscus*, were found at the exit of the slump, with ^{14}C ages of 4450 ± 35 and 8215 + 45/−40 ^{14}C yr BP, respectively. A third carcass—of a young horse (foal)—was collected in 2018 from the upper sand unit near the northeast margin of the slump headwall (Figure 8). The level of preservation was exceptional, with even the hair and soft tissue preserved. The foal's muscular system was radiocarbon dated to 39,850 ± 280 ^{14}C yr BP.[29]

4.4 | Plant and insect remains

Paleobotanical analyses of carpological remains (seeds) and pollen originating from the Batagay permafrost sequence cover the time span of the last about 120,000 yr BP.[17] Two samples rich in plant remains from the woody layer and upper sand, respectively, reveal the detailed composition of paleovegetation of the Last Interglacial (LI, stratigraphically attributed) and onset of the Last Glacial Maximum (LGM, dated to 26,180 yr BP).[17,20] Both pollen and plant macrofossil analyses reveal the presence of light coniferous taiga with a larch

FIGURE 6 Stratigraphic units exposed in the headwall (about 50 m high) of the Batagay megaslump, May 12–13, 2016. Photographs © J. B. Murton
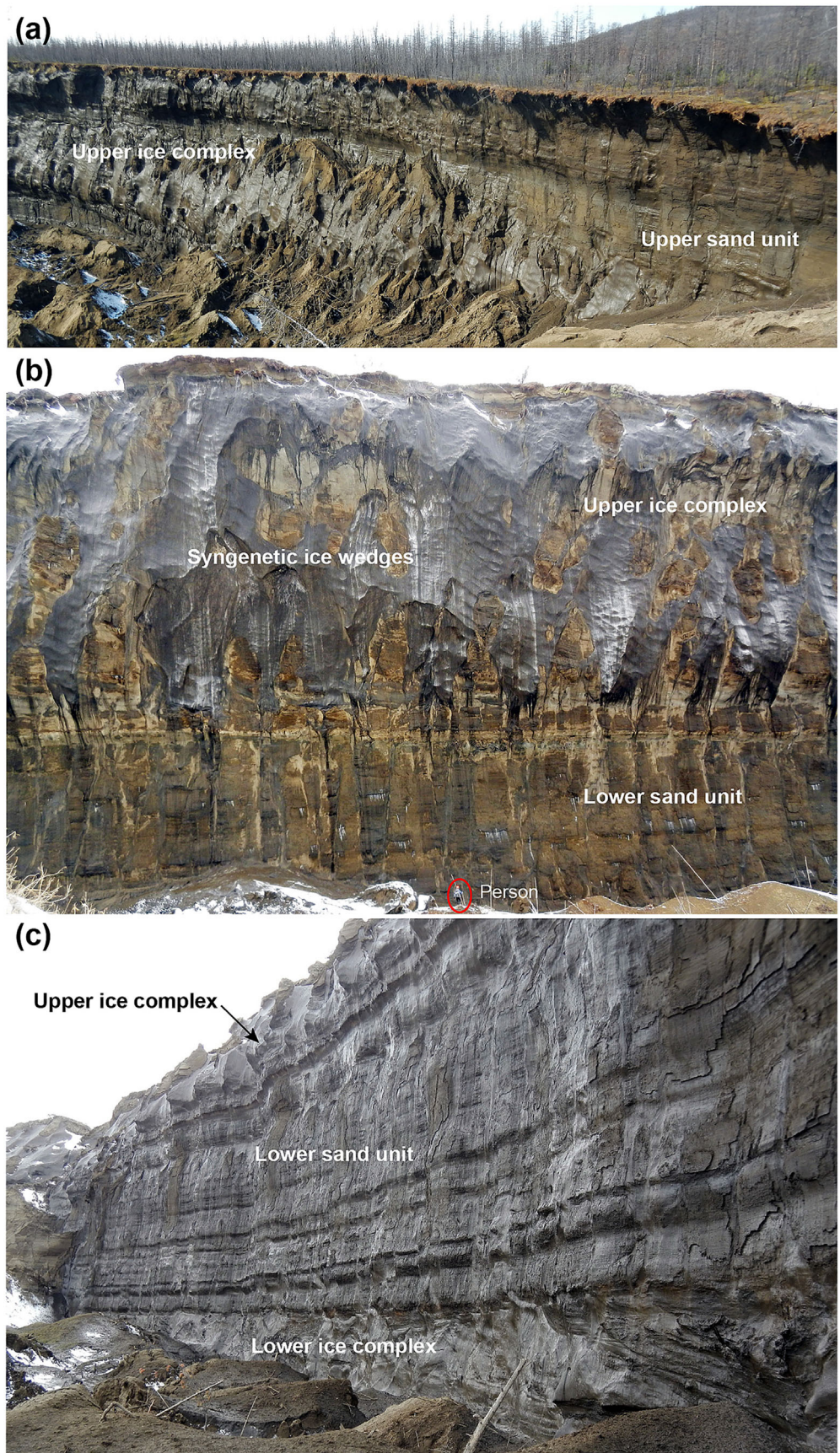
TABLE 1 Cryostratigraphic units identified at the Batagay megaslump

Unit and approximate thickness (m)	Comments	Interpretation	Preliminary age*
7. Near-surface sand (1–3)		Colluvium	MIS 1 (Holocene)
6. Upper sand (20–30)	Thickens downslope	Eolian sand sheet with reworking by slopewash	MIS 3–2
5. Upper ice complex (20–25)	Yedoma	Growth of large syngenetic ice wedges	MIS 4–3
4. Woody debris (≤3)	Discontinuous and cuts down into lower sand unit	Forest bed above erosional surface (disconformity)	MIS 5e (last interglacial)
3. Lower sand (≤20)		Eolian sand sheet with forest bed near top	MIS 6 or older
2. Lower ice complex (3–7)		Growth of large syngenetic ice wedges; forest bed	MIS 16
1. Diamicton (≥0.5)		Colluvium, locally derived from bedrock	MIS 16 or older

Note: Based on Ashastina et al.,[20] Murton et al.,[4,12] Opel et al.,[21] and Vasil'chuk et al.[22,23] See text, Figure 13 and Murton et al. (2022,[4] figure 2) for descriptions of stratigraphic relationships between upper ice complex and upper sand in different locations along the perimeter of the megaslump.
*MIS: Marine Isotope Stage.
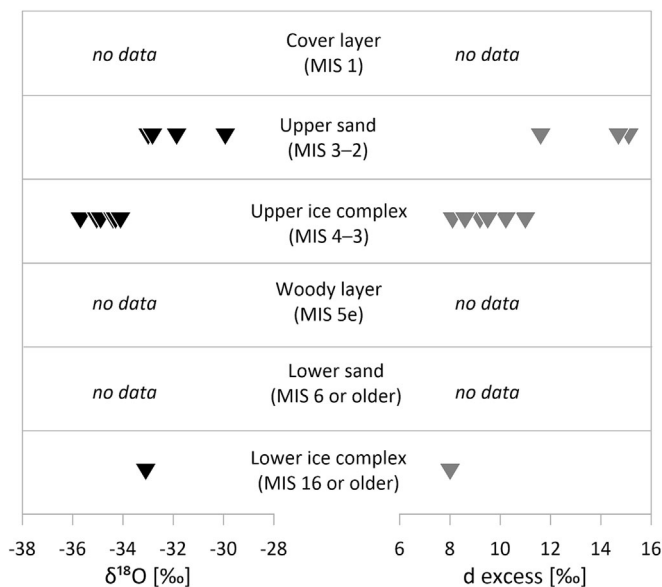
FIGURE 7 Mean ice-wedge $\delta^{18}O$ and d-excess values for the lower ice complex, the upper ice complex, and the upper sand units[21,24,25]

(*L. gmelinii*) canopy and an understorey of birch (*Betula* sp.), shrub alder (*Alnus* subg. *Alnobetula*), pine (*Pinus* subg. *Diploxylon*), and spruce (*Picea* sp.) during the LI (Figure 9). Remains of this taiga forest are assumed to be preserved in the woody layer. A large number of charred seeds and charcoal fragments indicate wildfire events that created clearances in the larch forest; numerous remains of xerophilous plants indicate the presence of steppe vegetation dominated by forbs (*Festucetalia lenensis*).

Pollen and plant macrofossils indicate that pre-LGM vegetation was mainly composed of steppe plants (e.g., *Artemisia* sp., *Silene* sp., *Festuca* sp., *Koeleria* sp., and *Stellaria* sp.), open-ground vegetation (e.g., *Plantago canescens*, and *Papaver* sect. *Scapiflora*) and larch trees. An almost absence of taiga plants and a high abundance of steppe vegetation indicate that climatic conditions pre-LGM were drier than during the LI. Modern plant communities near Batagay that largely resemble the LI and LGM vegetation reconstructions are shown in Figure 9a and b, respectively.

According to paleovegetation reconstructions, the Batagay area was covered with meadow—steppes along with groves of cold-deciduous trees (mainly larch) throughout most of the Late Pleistocene. However, the percentages of taiga and open vegetation in the total vegetation cover changed through time in response to fluctuating climatic conditions and the degree of disturbance by wildfires and herbivores. Late Pleistocene vegetation typical of coastal lowlands—cold-resistant tundra–steppe communities with *Kobresia myosuroides* or *Dryas* sp.[30–34]—was scarce at the Batagay site during the Late Pleistocene. This may have been induced by the extreme continental climate of the region—low precipitation and a large annual temperature range.

Entomological analysis of chitin remains found in the Batagay permafrost sequence supports the interpretation of paleovegetation reconstruction and adds data to our understanding of the paleoecological conditions at the site. A high abundance of sclerites belonging to the carpenter ant *Camponotus herculeanus* and fragments of the rove beetle genus *Atheta* (which inhabits mushrooms) in the samples of LI age indicate the presence of complex taiga forest at the site. Inhabitants of forest glades and cold and dry steppes were also detected in the sequence: the weevil *Phyllobius virideaeris*, the pill beetle *Morychus viridis* (Figure 10), the leaf beetle *Chrysolina arctica*, and the weevil *Otiorhynchus cribrosicollis*. In the pre-LGM layer typical meadow and meadow–steppe insects were identified: *Anthicus ater* and *Phyllobius kolymensis*. The Late Pleistocene part of the Batagay sequence also contains aquatic and riparian insects (e.g., *Ephemeroptera* sp., *Trichoptera* sp., *Saldula* sp., *Daphnia* sp.) and abundant finds of a cold-steppe species of pill beetle, *Morychus viridis*. This is a modern endemic of northeastern Siberia, occurring in relict, cold, very dry, exposed, and snowless steppes.[35,36] *Morychus viridis* is also characteristic of the Pleistocene mammoth steppe in Western
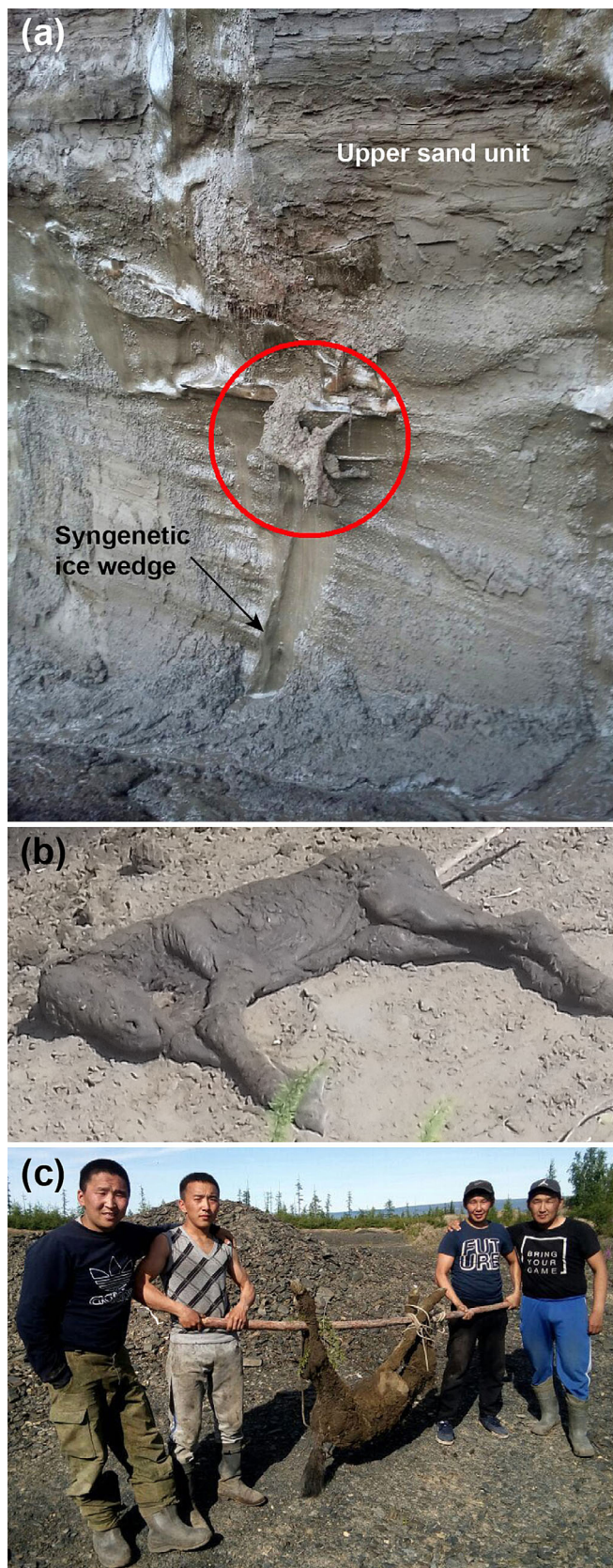
FIGURE 8 Foal carcass obtained in 2018 from permafrost deposits exposed in the headwall of the Batagay megaslump. (a) Carcass in situ (in center of red circle) within the upper sand unit, shortly before it fell onto the slump floor. Location is near the right side of Figure 6a. (b) Newly found carcass soon after thaw release from permafrost. (c) Carcass some hours later, when its color had changed to brown. Photographs © G. N. Savvinov (b) and other authors (a, c)

Beringia and found in the majority of northeast Siberian fossil assemblages.[36]

Entomological remains of the Batagay permafrost sequence indicate that the site was mainly inhabited by steppe insects, while tundra species were scarce: the Arctic tundra invertebrate group is absent here, the wet tundra group comprises less than 2%, and the portion of the dry tundra group ranges between 1 and 7%.[17] By contrast, the proportion of tundra invertebrates in permafrost sequences of the coastal lowlands reaches 80%.[37]

The assemblages of plant macro- and microfossils together with invertebrate remains reveal fewer tundra taxa during the Late Pleistocene at the Batagay site than records from the present coastal areas.[30–32,34,37]

4.5 | Ancient DNA and biomarkers

In a pilot study, Courtin et al.[38] applied shotgun metagenomic analyses of sedimentary ancient DNA to infer past glacial and interglacial ecosystem-wide biotic composition from ancient permafrost of the Batagay megaslump. Complementary pollen and plant metabarcoding data from the same samples largely confirm the main results. Two samples from the lower ice complex and the lowermost part of the lower sand indicate interglacial ecosystems assigned to MIS 17 and 7, respectively. These ecosystems were characterized by forested vegetation (*Pinus*, *Betula*, *Alnus*), open grassland, and at least intermittent water bodies, with birds and small omnivorous mammals. Microbial and fungal communities indicate substantial soil decomposition. A sample of the upper ice complex revealed cold–temperate grassland vegetation with episodic water bodies during MIS 3. The fauna was dominated by a diverse megafauna (*Mammuthus*, *Equus*, *Coelodonta*) and small mammals (rodents). Harsher conditions with cold-adapted herbs and typical Pleistocene megafauna have been reconstructed from two samples of the upper sand dated to MIS 2, supporting the paleovegetation reconstruction based on plant remains.[17]

In a study of fossil biomolecules, Jongejans et al.[39] differentiated organic matter preservation of glacial and interglacial periods by analyzing biomarkers (alkanes, fatty acids, and alcohols). Similar biogeochemical signatures with terrestrial characteristics and indications of limited microbial activity were deduced for glacial periods represented by the lower and the upper ice complex units and the lower sand unit. In contrast, the *n*-alkane and fatty acid distributions for interglacial periods (i.e., the woody layer and the Holocene cover) indicate higher microbial organic matter decomposition.[39]
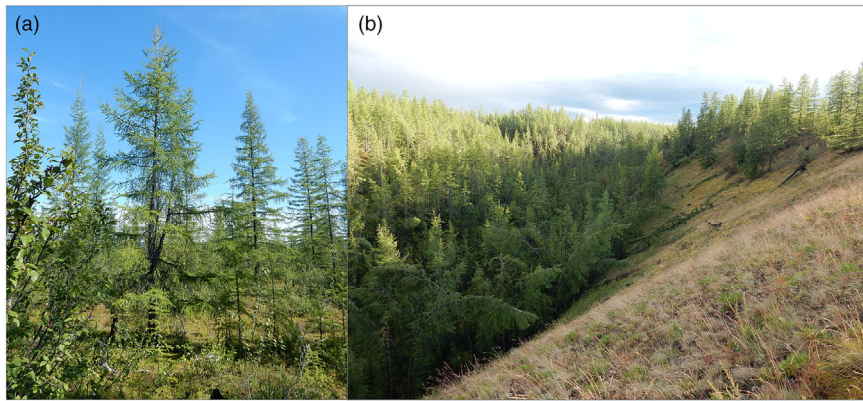
FIGURE 9 Modern plant communities in the vicinity of the Batagay site resembling LI (a) and pre-LGM vegetation (b). (a) Open *Larix gmelinii* forest with *Alnus fruticosa*, several *Betula* sp., *Salix* sp., *Equisetum scirpoides*, *Empetrum nigrum*, *Vaccinium vitis-idaea*, and *Pyrola* sp.; (b) steppe communities on a south-facing slope with *Alyssum obovatum*, *Potentilla* sp., *Stellaria* sp., *Artemisia* sp., *Festuca* sp., *Koeleria* sp., *Poa* sp., and *Thymus serpyllum*
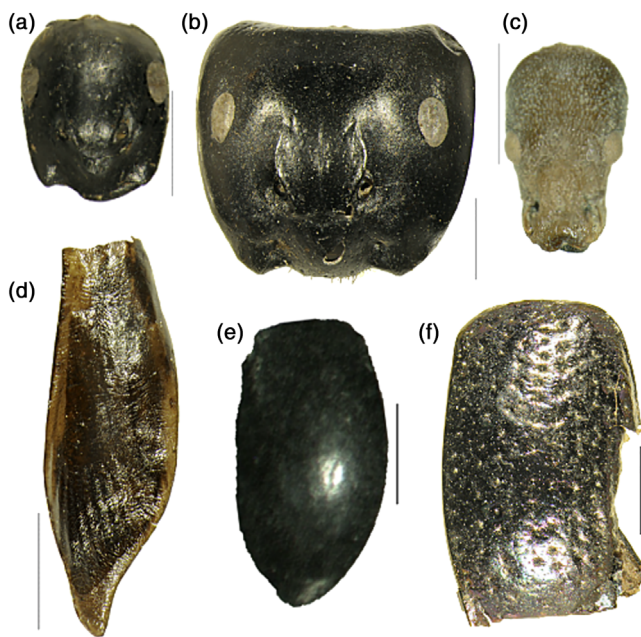
FIGURE 10 Selected invertebrate sclerites from the Batagay samples: (a) head of minor worker of *Camponotus herculeanus*; (b) head of major worker of *C. herculeanus*; (c) head of *Phyllobius kolymensis*; (d) wing pad of Ephemeroptera gen. indet.; (e) elytron of *Morychus viridis*; (f) elytron of *Chrysolina arctica*. Photographs a–d and f are from S. Kuzmina, while photo e is from V. Boeskorov

4.6 | Pleistocene and Holocene environmental history

The Quaternary environmental history of the Batagay slump site has been reconstructed from reconnaissance studies[4,12,17,20–25,38–40] and awaits systematic investigation. In essence, the preliminary reconstruction is thought to record the interaction of colluvial, eolian, and permafrost processes on a hillslope episodically forested during the last 650 ka or more. Below we summarize the history based on the seven stratigraphic units:

1. The diamicton at the base of the sedimentary sequence is interpreted as colluvium deposited by solifluction and related processes that locally reworked frost-shattered slate downslope. The broad age is probably Middle Pleistocene or older, though the exact age is unknown.

2. Woody material related to erosional features in the overlying lower ice complex is interpreted as remains of an interglacial forest bed, possibly dating from the penultimate interglacial, during MIS 7, about 243–190 ka. An older age, however, cannot be discounted because the lower ice complex (with its syngenetic ice wedges that formed under cold but moist conditions) has been preliminarily dated to MIS 16.

3. The lower sand unit is thought to represent eolian sand-sheet deposits that formed under dry conditions. Rapid deposition is inferred from the narrow and tall composite wedges. The middle of the unit has provided luminescence ages of 210 to >123 ka, suggesting deposition during MIS 6 or 7. Again, an older age for the so far undated lower part of the unit cannot be ruled out.

4. The woody debris unit is interpreted as a second forest bed, probably dating from the last interglacial (MIS 5e), about 132–117 ka. This represents the oldest Late Pleistocene unit. According to paleobotanical analysis, meadow–steppe vegetation filled openings in the dry, herb-rich light coniferous taiga that experienced wildfires. The woody debris related to erosional features may have accumulated within paleostreams or channels after an episode of erosion during which the top of the underlying lower sand unit was gullied, probably by thermal erosion.

5. The upper ice complex was associated with the growth of large syngenetic ice wedges, formed as result of a substantial increase in snow melt water supply into thermal contraction cracks relative to the limited water supply to the narrow composite wedges in the lower and upper sand units. Radiocarbon ages from this ice

complex range from nonfinite through 48 ka to about 23 ka ^{14}C BP, which point to an MIS 3 age, perhaps extending back into MIS 4. This period was characterized by extremely continental climate conditions, as inferred from ground-ice stable isotopes and vegetation reconstruction. Meadow–steppe vegetation with tundra–steppe inclusions, mostly dry and exposed ground, and the presence of ephemeral small ponds were characteristic for this accumulation period.

6. The upper sand unit has provided ^{14}C ages of about 38–19 ka ^{14}C BP, as well as nonfinite ages. In addition, on stratigraphic grounds we suggest that an age of about 13 ka ^{14}C BP assigned by Ashastina et al.[20] to the upper ice complex is actually from the upper sand unit. Collectively, the ^{14}C ages from the upper sand unit suggest deposition of eolian sand during MIS 3–2, at least in places at the same time as the formation of the upper ice complex, and again possibly extending back further. Typical for this unit with narrow composite wedges was meadow–steppe vegetation with exposed ground and scattered larch stands with ephemeral ponds or paddles.

7. The near-surface layer of sand probably developed by a combination of thaw truncation of the underlying upper ice complex, colluvial processes, and soil formation. A Holocene age is likely.

Overall, exposed floodplains of proximal rivers such as the Batagay and Yana, within 2 and 10 km, respectively, of the slump are the assumed major source of the sediments exposed in the slump, which implies upslope directed transport by wind. Another potential source of sand is the Pliocene Tabalakh Suite that underlies the upland to the northeast of the Batagay River valley. Periglacial and nival processes on hillslopes near the slump may also have contributed to sediment supply during the Pleistocene and Holocene.

5 | RECENT MEGASLUMP DEVELOPMENT

5.1 | Chronology

Following disturbance of the vegetation and soil, the megaslump developed in three stages: (1) gully initiation and growth, (2) transition to a thaw slump, and (3) development of more complex, megaslump morphology. The stages can be reconstructed from a time series of satellite images that show landform development between 1962 and 2018 on the northeast-facing hillslope below the col between mounts Kirgilyakh and Khatyngnakh (Figure 11). The images were used by Savvinov et al.[41] to measure landform area and geometry through time (Figure 12).

The rate of areal growth of the landform from hillslope gully through thaw slump to megaslump has been remarkably uniform (Figure 12). Just one distinct inflexion is apparent during the early 1980s, when the growth rate increased somewhat during the transition from gully to thaw slump. Overall, the uniform growth rate of the slump is consistent with general monotonic increases in summer air temperature and summer precipitation shown in Figure 3c and d.

Disturbance to vegetation and soil resulted from deforestation and off-road vehicle activity.[41] Deforestation and export of timber to nearby settlements and facilities of Dalstroy (Far North Construction Trust) during the 1940s and 1950s were carried out by inmates of the Yansky Forced Labour Camp (Yanglag). Today, evidence for tree clearance persists on the hillslope, as numerous old tree stumps. Around the same time as trees were cut, heavy tracked vehicles crossed the hillslope, as the Yansky Mining and Industrial Administration of the Dalstroy Trust began exploring for tin, gold, and other minerals. Exploration activity intensified after 1963 under the organization of the Yansky Exploration Expedition. A tin mine, now inactive, was developed near Mount Kirgilyakh. Overall, tree cutting reduced interception storage by vegetation and thus probably increased surface runoff, while passage of tracked vehicles probably damaged and compressed the near-surface organic layer, causing the active layer to deepen. These mechanical and thermal disturbances then set in train a series of thermokarst processes that resulted in megaslump development.

In stage 1, a gully initiated and extended across the hillslope (Figures 4 and 11). By 1962, the gully was more than 800 m long and about 30 m wide along the thalweg, and traversed what is now the center of the megaslump. The gully is visible on satellite images from 1962, 1968, 1975, and 1980 (Figure 11a–d), and appears to have widened, at least in its central part, during this period. As recently as 2018, the uppermost several hundred meters of the gully persisted on the hillslope above the slump, and the gully was truncated on its downslope side by the central top part of the slump headwall (Figure 11l), forming a distinctive notch in the headwall profile.

Stage 2 commenced with the transition from gully to thaw slump during the 1980s and was followed by rapid growth of the slump. The transition probably began when erosion reached the upper ice complex, whose high ice content made it susceptible to thermokarst activity and provided a major source of meltwater to wash away thawed material. By 1991, the central part of the gully had developed convex-outward sides, creating a bulbous form in plan view (Figure 11e). Such a form is characteristic of thaw slumps, which typically have arcuate headwalls. Since 1991, the slump has grown substantially wider and longer (Figure 11e–l;[42–44]).

Stage 3 began with the transition to a megaslump (i.e., area >20 ha) since the 1990s (Figure 11e,f). Slump growth was rapid, attaining an area of almost 77 ha by 2018 (Figure 12;[41]), respectively about 80 ha in 2019.[18] Major expansion of the megaslump occurred between 2010 and 2014, before the expansion unexpectedly slowed down.[44] The height of the headwall has been measured as up to 51.7 m in 2016[12] and up to 55 m in 2019.[18] Slump growth has involved the processes of ablation of ice in the headwall, thermal erosion of the headwall and slump floor, and permafrost degradation beneath the floor. The slope of the central channel across the slump floor is concave.[18] The channel evacuates some sandy sediment from the slump floor into the adjacent Batagay River, though the rates and volumes remain to be determined.

Based on the development of the Batagay megaslump over just several decades, as outlined above, it is clear that the Batagay megaslump is a prime example of rapid or abrupt permafrost thaw.[45] In
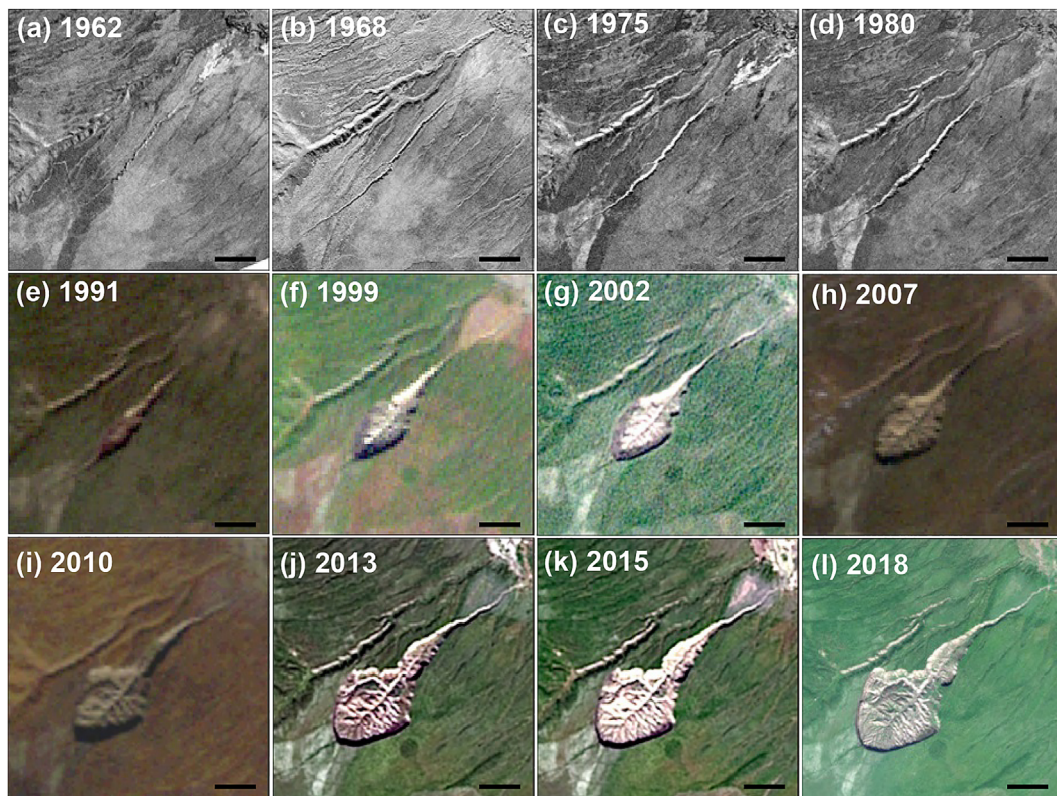
FIGURE 11 Time series of satellite images of the Batagay hillslope gully and thaw slump between 1962 and 2018. Scale bar on all images represents about 400 m. Images provided by Victor Makarov and Aleksey Petrov. Modified from Savvinov et al[41]

contrast to gradual permafrost thaw, abrupt permafrost thaw such as the development of the Batagay megaslump and related greenhouse gas emissions are not accounted for in climate models.[46]
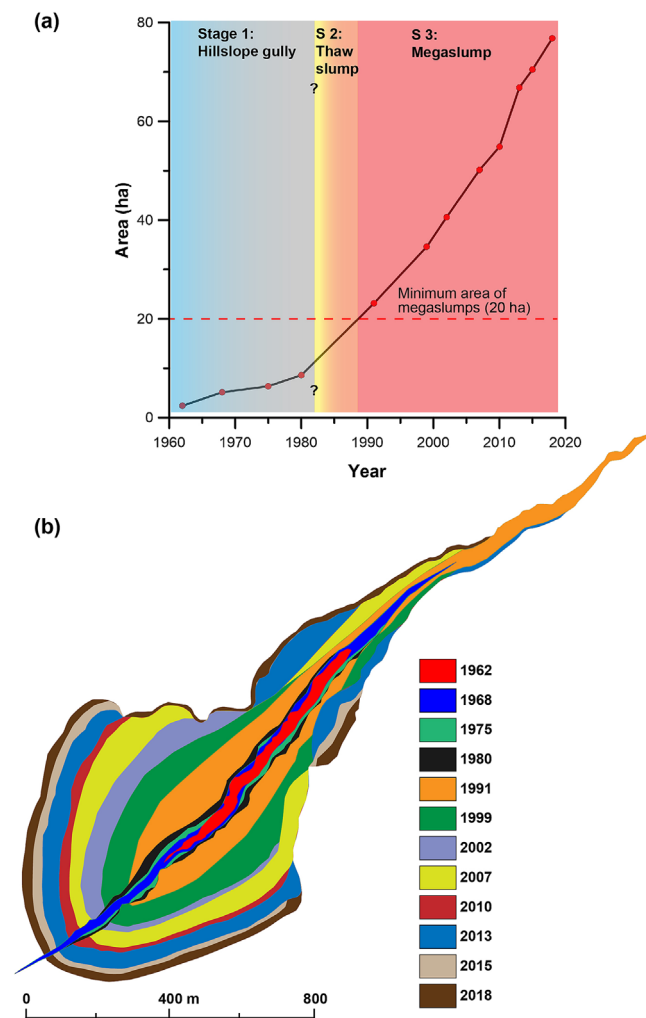
5.2 | Headwall ablation

Headwall ablation occurs by solar radiation and sensible heat transfer, leading to ground-ice melt, permafrost thaw, and thus rapid slope retreat. Retreat rates depend on diurnal and seasonal weather conditions, ground-ice distribution and slump geometry. The high ice content of the permafrost deposits exposed in the slump—reaching up to 87 vol% in the upper ice complex unit—favors high rates of headwall retreat.[18] Based on the distribution of the exposed cryostratigraphic horizons the headwall can be subdivided into three types of slope: (a) a vertical slope with only a slight inclination in the upper part, (b) a two-part slope with an inclined upper part and a steep lower part, and (c) a two-part slope with a concave steep (but not vertical) upper part and a flattened lower part.[18] Rapid ablation in thaw slumps is generally favored by clear, warm, and windy conditions, when radiative inputs and turbulent transfer of heat to the frozen ground and the ice are high, and during rainstorms, which wash thawed sediment from the thaw face. Ablation due to solar radiation occurs even in spring with air temperatures below $-10°C$, but is of course strongest in summer and autumn. Headwall ablation causes sand and organic material fall, slide, or flow onto the slump floor, where they are reworked by debris flows near the foot of the headwall or by meltwater. Limited debris-flow activity occurs near the foot of the headwall as the sand tends to drain quickly and so favors rapid channeling of water into gullies that dissect the slump floor.

5.3 | Thermal erosion

Thermal erosion occurs where flowing water melts ground ice by the combined effects of heat conduction and convection, and then mechanically erodes newly released sediment.[47] Thermal erosion of ice-rich permafrost can form gullies.[48,49] The main source of water is melting ground ice exposed in the headwall and along the sides of slump-floor gullies during summer. Additionally, spring snowmelt and summer rainstorms may contribute episodically to discharge. Discharge is greatest during snowmelt, hot summer days, or rainstorms. The fine sediment eroded and suspended within turbulent ephemeral streams on the slump floor colors the water dark gray. Bedload comprises pebble- to cobble-sized clasts reworked from Quaternary sediments and eroded from the slate bedrock. The sediment released from the slump episodically dams the Batagay River, forming a temporary lake that drains abruptly.

FIGURE 13 Gullies and interfluves form a topography of icy badlands in the slump floor, July 29, 2017. Accordant summits of interfluves indicate the base of the upper ice complex, marked by a solid white line (where the top is exposed in the headwall) and by a dashed white line (where it is extrapolated). Blue line marks the contact between top of upper ice complex and base of upper sand unit. Location of the main gully is indicated. Mount Khatyngnakh in background. Photograph © J. B. Murton

FIGURE 12 Growth of gully–slump system between 1962 and 2018. Time series of landform area (a) and landform outlines (b). Modified from Savvinov et al[41]

FIGURE 14 The primary gully in the slump floor. (a) Active section with stream flowing, May 13, 2016. (b) Stabilized sides on both sides of the primary gully in the slump exit, July 29, 2017. Photographs © J. B. Murton

Thermal erosion on the floor of the thaw slump has formed a striking topography of icy badlands (Figures 5 and 13). In cross-profile, the badlands comprise v-shaped gullies between sharp-crested interfluves. Active gully sides commonly expose bare sand, often at or near the angle of repose of the sand, due to active mass movement. A general accordance in height of the summits of the interfluves as well as baydzherakhs (sedimentary thermokarst mounds remaining after ice-wedge melt) on top of the interfluves initially mark the base of the upper ice complex, though erosion progressively lowers them through time. The original hillslope gully (Figure 11a–c) now forms the primary gully that runs downslope along the middle of the slump floor towards the Batagay River (Figures 5, 13, and 14). Tributary gullies feed into the main gully in an orthogonal pattern (Figure 5). In summer, thermo-erosional niches commonly develop beside active streams in gully floors.

5.4 | Permafrost degradation beneath the slump

Permafrost degradation beneath slump floors occurs by heat conduction and/or convection. Where slump-floor sediments are rich in silt and clay, impeding percolation of water, degradation occurs mainly by conductive heat flow.[50] No measurements of permafrost degradation beneath the slump floor at Batagay have been reported. It is likely, however, that convective heat flow from percolating water contributes substantially to thaw because the sediments contain abundant sand.

5.5 | Slump stabilization

Thaw slumps eventually stabilize if their site is not eroded away. Stabilization results when all of the excess ice has melted, where slumped soil and vegetation insulate the headwall, or where the slope gradient above the headwall is less than that of the slump-floor deposits, which therefore bury the excess ice. The duration of thaw slumping varies from a single summer to at least several decades.[50,51] After slumps stabilize, permafrost may re-aggrade beneath the slump floor and vegetation re-establish. Where erosion episodically removes slumped debris, thaw slumping may be reactivated, producing cycles of slumping and stability. Evacuation of slump debris, for example by heavy rainfall, can perpetuate slump growth.[52] In the case of the Batagay slump, parts of the slump have stabilized while others are actively slumping, in particular the central part of the headwall. In addition, two secondary headwalls have developed in a former stabilized part of the slump, near the exit. Local stabilization of the slump floor has occurred where slopes have declined in angle and shrubby and herbaceous vegetation has grown back, which characterizes much of the downslope several hundred meters of the slump, near the exit (Figure 14b). However, revitalization of erosion through secondary failure of material in the scar zone is another possibility.

5.6 | Future development

The Batagay megaslump is likely to grow wider and longer before eventually stabilizing.[18] Observations of the ground-ice stratigraphy and rates of headwall retreat over recent years suggest that the current expansion will continue for at least the next several years to decades but will be spatially limited by the distribution of near-surface ice-rich sediments up the hillslope. Over the next few years or more, the most active part of the slump will almost certainly unite with the separate gully to the north of the slump, which may change the slump dynamics. The icy badlands terrain in the slump floor are likely to become progressively more muted as erosion and deposition tend to promote slope decline. Local reactivation of parts of the slump floor and sides, however, are likely to follow high-magnitude erosion events, for example triggered by intense summer rainfall or rapid snowmelt. Ultimately, the terrain will not recover its initial pre-disturbance form, because this would require renewed growth of an ice complex to form new ice-rich permafrost, which last occurred during the Pleistocene. Instead, the terrain is likely to assume an irregular form characterized by sandy ridges and sand-filled elongate depressions formed by the degradation of the icy badlands.

6 | COMPARISON WITH OTHER MEGASLUMPS

Comparison of the Batagay megaslump with megaslumps elsewhere reveal a number of similarities and differences in terms of their geomorphology, permafrost deposits, and Quaternary history. To date, about 10 megaslumps have been reported in addition to the Batagay megaslump, from the Peel Plateau, Richardson Mountains, and eastern foothills of the Mackenzie Mountains, NT, Canada.[3,52,53]

Similarities between the Batagay and Canadian megaslumps include the following. First, geomorphic coupling between hillslope and fluvial systems has been facilitated by megaslump development. Slumping has transferred large amounts of detrital and dissolved materials into nearby streams and can shift systems from fluvial incision to floodplain aggradation/valley infilling.[53] All megaslumps export large volumes of sediment into adjacent river systems such as the Peel and Willow rivers in Canada and the Batagay River in Siberia. Increased suspended sediment and bedload transport in the rivers are visually obvious; dissolved loads have also increased in the Canadian rivers, but results remain to be published from Batagay. Second, initiation of slumps has tended to relate to the development of stream networks and fluvial processes, for example along gullies or water tracks following heavy rainfall (Figure 15a).

Differences between the Batagay and Canadian megaslumps are also evident. First, the Batagay megaslump development is closely linked to the existence and distribution of ice-complex deposits, whereas the Canadian megaslumps have all developed in terrain glaciated by the Laurentide Ice Sheet during MIS 2. Glaciation deposited glacial sediments and buried basal glacier ice. For example, beneath the Peel Plateau, superficial deposits up to 60 m thick and of glacial, glaciofluvial, and glaciolacustrine origin overlie Cretaceous shale and siltstone (Figure 15). As a result of glaciation and erosion of older Quaternary deposits, the superficial deposits of the Peel Plateau are thought to be much younger (MIS 2) than those of the unglaciated terrain around Batagay (since MIS 16). Second, the sediment properties differ substantially. Cohesive, fine-grained (clay- and silt-rich) deposits, for example in tills, dominate the Canadian megaslumps. As a result, the permeability of newly thawed sediments is relatively low, limiting drainage and generating extensive debris flows on slump flows and sometimes extending into adjacent river valleys (Figure 16). In contrast, noncohesive (granular) sandy deposits dominate at Batagay, and their higher permeability expedites drainage and so suppresses debris-flow activity on the gentle slump floor. Instead, thermal erosion dominates the floor of the Batagay megaslump, producing icy badlands (Figures 5, 13, and 14). Thus, slump morphology differs, with the highly gullied floor at Batagay contrasting with the flatter, more boxlike slump floors on the Peel Plateau.
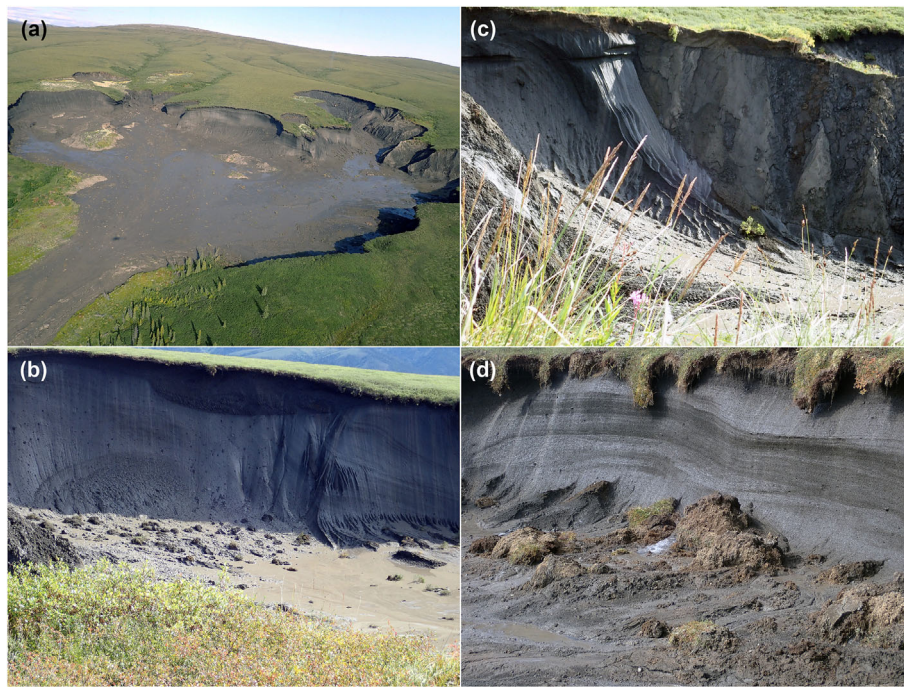
FIGURE 15 Willow River megaslump, Peel Plateau, NT, Canada, August 8, 2019. (a) Oblique aerial photograph of megaslump, showing a complex and irregular slump morphology with multiple arcuate sections of headwall and shallow drainage lines ("water tracks") upslope of the slump. (b) Massive icy diamicton with numerous cobbles protruding from headwall; unconformably overlain by diamicton. (c) Massive icy diamicton, sand, and diamicton. (d) Recumbent isoclinal folds in massive icy diamicton. Photographs © J. B. Murton
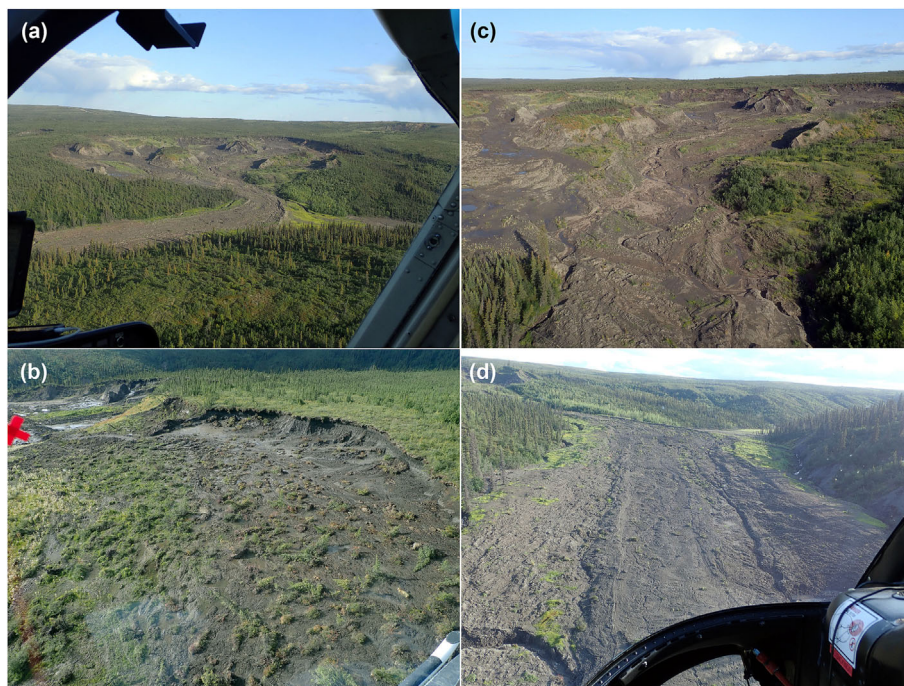
FIGURE 16 Fort McPherson 2 megaslump/FM2 (informally named by Kokelj et al. 2015[52]), Peel Plateau, NT, Canada, August 8, 2019. (a) Oblique aerial photograph of slump and track of debris-flow deposits leading downslope and partially infilling a valley. (b) Active debris flows on slump floor. Massive icy sediments exposed in headwall. (c) Largely inactive debris flows leading out of slump into adjacent valley. (d) Valley partially infilled with slump-generated debris-flow deposits. Entrance to slump in top left. Note lower level of unfilled part of a valley in upper right. Photographs © J. B. Murton

Third, permafrost development has differed fundamentally between the Canadian and Siberian sites, being epigenetic at the former and syngenetic at the latter. Hence, Batagay permafrost preserves a very long record of environmental and climatic change, whereas the Peel Plateau permafrost provides a snapshot of the last Laurentide glaciation/early deglaciation. Fourth, the size and number of active megaslumps have increased substantially in recent decades in the Peel Plateau due increasing magnitude and intensity of summer rainfall, while summer air temperatures have remained stable.[52] These contrast with the more uniform rate of growth of the Batagay slump (Figure 12) and small increases in summer rainfall and summer air temperature (Figure 3c and d). Fifth, buried, relict thaw slumps are relatively common in the Canadian context, and newly initiated thaw slumps commonly erode into the remains of much older slumps (J. Tunnicliffe, pers. comm. 2023). This does not appear to be the case for the Batagay megaslump. Lastly, human triggering of slumping clearly applied to the Batagay megaslump, whereas this does not seem to be the case of the Canadian megaslumps.

Both the Canadian and Batagay megaslumps have been highly active and rapidly evolving in recent decades. Average retreat rates of headwalls obtained for three Canadian megaslumps over a 20-year period from 1990 to 2010 were 9.4, 15.0 and 26.7 m yr^{-1}.[3] Lacelle et al.[3] reported that for all of the thaw slumps observed in their study (0.54–52 ha in area; i.e., including ordinary thaw slumps as well as megaslumps), the largest slumps tended to show the highest retreat rates. These authors also suggested that the Canadian megaslumps generate feedbacks that enable their growth to perpetuate and maintain growth rates considerably greater than those of smaller slumps. For comparison, rates of headwall retreat for the Batagay megaslump were calculated as 7–15 m yr^{-1}year in 2004–2010 in different parts of the headwall,[43] 10.3 ± 3.7 m yr^{-1} for 2006–2016,[42] and 11.3–14.9 m yr^{-1} in 1991–2018 (area loss data in Vadakkedath et al. 2020[44] recalculated in Kizyakov et al. 2023[18]).

In terms of the relative amount of geomorphic "work" being accomplished at the Canadian and Batagay megaslumps, the inventory of Yakutian thermoerosional features has yet to be determined. This inventory is needed to establish the relative importance of the Batagay megaslump in exporting sediment and carbon and in shaping the landscape. Qualitatively, we note that the turbid meltwater streams on the slump floor collectively export large volumes of sandy sediment in the adjacent Batagay River, which appears to result in fluvial aggradation downstream of the meltwater input. In the Canadian case, the sediment budget for Stony Creek and Willow River is now dominated by just a few, very large features.[52,53]

7 | CONCLUSIONS

The Batagay megaslump is exceptional in two respects. First, it provides unique access to ancient permafrost and offers enormous potential to reconstruct paleoenvironmental conditions and to study past climate–permafrost interactions since the Middle Pleistocene. Second, it demonstrates the high sensitivity of ice-rich permafrost to abrupt thaw as a result of terrain disturbance. Disturbance of the taiga vegetation and organic layer by human activity initiated thermokarst activity, first in the form of hillslope gullying and then as thaw slumping. Slump growth probably accelerated due to climate warming and wetting. In geomorphic terms, the site provides an excellent opportunity to study rapid thermokarst landscape development over decadal timescales and its impact on solutes and suspended sediment concentrations in rivers downstream of the slump. Such study is important to understand how other deepened gullies and initial slumps near Batagay may affect the terrain and ecosystems under conditions of continued global warming, increases in summer rainfall, and frequent wildfires.

DATA AVAILABILITY STATEMENT

The data that support the findings of this study are openly available in University of Sussex at http://www.sussex.ac.uk/geography/resources/labs/permafrost.

ORCID

Julian Murton https://orcid.org/0000-0002-9469-5856
Thomas Opel https://orcid.org/0000-0003-1315-8256
Sebastian Wetterich https://orcid.org/0000-0001-9234-1192

REFERENCES

1. Lewkowicz AG, Way RG. Extremes of summer climate trigger thousands of thermokarst landslides in a high Arctic environment. *Nat Commun*. 2019;10(1):1329. doi:10.1038/s41467-019-09314-7
2. Burn CR, Lewkowicz AG. Retrogressive thaw slumps. *Can Geogr*. 1990;34(3):273-276. doi:10.1111/j.1541-0064.1990.tb01092.x
3. Lacelle D, Brooker A, Fraser RH, Kokelj SV. Distribution and growth of thaw slumps in the Richardson Mountains–Peel Plateau region, northwestern Canada. *Geomorphology*. 2015;235:40-51. doi:10.1016/j.geomorph.2015.01.024
4. Murton JB, Opel T, Toms P, et al. A multi-method dating study of ancient permafrost, Batagay megaslump, East Siberia. *Quat Res*. 2022;105:1-22. doi:10.1017/qua.2021.27
5. BBC Reel. Siberia's enormous hole in the ground is getting bigger. 18 January 2021. 2020. https://www.bbc.com/reel/video/p08lmh4z/siberia-s-enormous-hole-in-the-ground-is-getting-bigger
6. BBC Earth. In Siberia there is a huge crater and it is growing at an alarming rate. 2017. Date Accessed: 18 January 2021. http://www.bbc.com/earth/story/20170223-in-siberia-there-is-a-huge-crater-and-it-is-getting-bigger

7. Glushkova OY. Late Pleistocene glaciations in North-East Asia. In: Ehlers J, Gibbard PL, Hughes PD, eds. *Quaternary Glaciations - Extent and Chronology: a Closer Look*. Developments in Quaternary Sciences. Elsevier; 2011:865-875. doi:10.1016/B978-0-444-53447-7.00063-5

8. Toro J, Miller EL, Prokopiev AV, Zhang X, Veselovskiy R. Mesozoic orogens of the Arctic from Novaya Zemlya to Alaska. *J Geol Soc*. 2016;173(6):989-1006. doi:10.1144/jgs2016-083

9. Parfenov LM, Prokopiev AV, Gaiduk VV. Cretaceous frontal thrusts of the Verkhoyansk fold best, eastern Siberia. *Tectonics*. 1995;4(2):342-358. doi:10.1029/94TC03088

10. Stepanova NA. On the lowest temperatures on earth. *Mon Weather Rev*. 1958;86(1):6-10. doi:10.1175/1520-0493(1958)0862.0.CO;2

11. Ivanova RN. Seasonal thawing of soils in the Yana River valley, northern Yakutia. In: Phillips M, Springman SM, Arenson LU, eds. *Permafrost, proceedings of the eighth international conference on permafrost, 21–25 July 2003, Zurich, Switzerland*. Vol.1. A.A. Balkema; 2003: 479-482.

12. Murton JB, Edwards ME, Lozhkin AV, et al. Preliminary paleoenvironmental analysis of permafrost deposits at Batagaika megaslump, Yana uplands, Northeast Siberia. *Quat Res*. 2017;87(2):314-330. doi:10.1017/qua.2016.15

13. Hopkins DM, Matthews JV Jr, Schweger CE, Young SB (Eds). *Paleoecology of Beringia*. Academic Press; 1982.

14. Murton JB, Goslar T, Edwards ME, et al. Palaeoenvironmental interpretation of yedoma silt (ice complex) deposition as cold-climate loess, Duvanny Yar, Northeast Siberia. *Permafr Periglac Process*. 2015; 26(3):208-288. doi:10.1002/ppp.1843

15. Willerslev E, Davison J, Moora M, et al. Fifty thousand years of arctic vegetation and megafauna diet. *Nature*. 2014;506(7486):47-51. doi:10.1038/nature12921

16. Elias SA, Brigham-Grette J. Late Pleistocene glacial events in Beringia. In: Elias SA, Mock CJ, eds. *Encyclopedia of Quaternary Science*. Vol.2. Second ed. Elsevier; 2013:191-201. doi:10.1016/B978-0-444-53643-3.00116-3

17. Ashastina K, Kuzmina S, Rudaya N, et al. Woodlands and steppes: Pleistocene vegetation in Yakutia's most continental part recorded in the Batagay permafrost sequence. *Quat Sci Rev*. 2018;196:38-61. doi:10.1016/j.quascirev.2018.07.032

18. Kizyakov AI, Wetterich S, Günther F, et al. Landforms and degradation pattern of the Batagay thaw slump, northeastern Siberia. *Geomorphology*. 2023;420:108501. doi:10.1016/j.geomorph.2022.108501

19. Vdovina LG. SUNGE (State Unitary Mining and Geological Enterprise) 'Yanageology' report for additional geological study, revision and preparation for publication of the 'State geological map of the Russian Federation', 1:200 000 scale (new series), sheet Q-53-III, IV [Batagay, Ege-Khaya] in 1995–2001. Annexes 4 (symbols for the geological map) and 7 (symbols for the Quaternary units map). 2002.

20. Ashastina K, Schirrmeister L, Fuchs M, Kienast F. Palaeoclimate characteristics in interior Siberia of MIS 6-2: first insights from the Batagay permafrost mega-thaw slump in the Yana highlands. *Clim Past*. 2017;13(7):795-818. doi:10.5194/cp-13-795-2017

21. Opel T, Murton JB, Wetterich S, et al. Past climate and continentality inferred from ice wedges at Batagay megaslump in the northern Hemisphere's most continental region, Yana highlands, interior Yakutia. *Clim Past*. 2019;15(4):1443-1461. doi:10.5194/cp-15-1443-2019

22. Vasil'chuk YK, Vasil'chuk JY, Budantseva NA, Vasil'chuk AC. New AMS dates of organic microinclusions in ice wedges from the lower part of Batagay Yedoma, Yakutia. *Dokl Earth Sc*. 2020;490(2):100-103. doi:10.1134/S1028334X20020154

23. Vasil'chuk YK, Vasil'chuk JY. The first AMS dating of organic microinclusions in an ice wedge of the upper part of the Batagay Yedoma Megaslump (Yakutia). *Dokl Earth Sc*. 2019;489(1):1318-1321. doi:10.1134/S1028334X19110096

24. Vasil'chuk Y, Vasil'chuk J, Budantseva N, Vasil'chuk A. MIS 3–2 paleowinter temperature reconstructions obtained from stable water isotope records of radiocarbon-dated ice wedges of the Batagay ice complex (Yana upland, eastern Siberia). *Radiocarbon*. 2022;64(6):1403-1417. doi:10.1017/RDC.2022.60

25. Vasil'chuk YK, Vasil'chuk JY, Budantseva NA, Vasil'chuk AK, Trishin AY. Isotope-geochemical characteristics of the Batagay Yedoma (preliminary results). *Ark Antarkt (Arctic and Antarctic)*. 2017; 3:69-96.

26. Palkopoulou E, Baca M, Abramson NI, et al. Synchronous genetic turnovers across western Eurasia in Late Pleistocene collared lemmings. *Glob Chang Biol*. 2016;22(5):1710-1721. doi:10.1111/gcb.13214

27. Lord E, Marangoni A, Baca M, et al. Population dynamics and demographic history of Eurasian collared lemmings. *BMC Ecol Evo*. 2022; 22(1):126. doi:10.1186/s12862-022-02081-y

28. Novgorodov GP, Grigorev SE, Cheprasov MY. Prospective location of the mammoth fauna in the Yana River basin. [in Russian]. *Int J Applied Fundamental Res*. 2013;8:255-259.

29. Siberian Times. Extinct ancient foal in pioneering cloning experiment is older than initially believed. 2018. Date Accessed: 8 November 2022. https://siberiantimes.com/science/casestudy/news/extinct-ancient-foal-in-pioneering-cloning-experiment-is-older-than-initially-believed/

30. Kienast F, Schirrmeister L, Siegert C, Tarasov P. Palaeobotanical evidence for warm summers in the east Siberian Arctic during the last cold stage. *Quat Res*. 2005;63(3):283-300. doi:10.1016/j.yqres.2005.01.003

31. Kienast F, Tarasov P, Schirrmeister L, Grosse G, Andreev AA. Continental climate in the east Siberian Arctic during the last interglacial: implications from palaeobotanical records. *Glob Planet Change*. 2008; 60(3-4):535-562. doi:10.1016/j.gloplacha.2007.07.004

32. Kienast F, Wetterich S, Kuzmina S, et al. Paleontological records indicate the occurrence of open woodlands in a dry inland climate at the present-day Arctic coast in western Beringia during the last interglacial. *Quat Sci Rev*. 2011;30(17-18):2134-2159. doi:10.1016/j.quascirev.2010.11.024

33. Reinecke J, Troeva E, Wesche K. Extrazonal steppes and other temperate grasslands of northern Siberia—phytosociological classification and ecological characterization. *Phytocoenologia*. 2017;47(2):167-196. doi:10.1127/phyto/2017/0175

34. Wetterich S, Kuzmina S, Andreev AA, et al. Palaeoenvironmental dynamics inferred from late Quaternary permafrost deposits on Kurungnakh Island, Lena Delta, Northeast Siberia. *Quat Sci Rev*. 2008; 27(15-16):1523-1540. doi:10.1016/j.quascirev.2008.04.007

35. Berman DI. Modern habitats of the pill beetle Morychus viridis (Coleoptera, Byrrhidae) and reconstruction of the Pleistocene environment of the northeastern USSR. *Rep AN USSR*. 1990;310(4):1021-1023. (in Russian).

36. Sher A, Kuzmina SA. Beetle Records. Late Pleistocene of Northern Asia. In: Elias SA, ed. *Encyclopedia of Quaternary Science*. Vol.1. Elsevier; 2007:246-267. doi:10.1016/B0-44-452747-8/00275-1

37. Kuzmina SA. Quaternary insects and environment of northeastern Asia. *Paleontol J*. 2015;49(7):679-867. doi:10.1134/S0031030115070011

38. Courtin J, Perfumo A, Andreev AA, et al. Pleistocene glacial and interglacial ecosystems inferred from ancient DNA analyses of permafrost sediments 956 from Batagay megaslump, East Siberia. *Environ DNA*. 2022;4(6):1265-1283. doi:10.1002/edn3.336

39. Jongejans LL, Mangelsdorf K, Karger C, et al. Molecular biomarkers in Batagay megaslump permafrost deposits reveal clear differences in organic matter preservation between glacial and interglacial periods. *Cryosphere*. 2022;16(9):3601-3617. doi:10.5194/tc-16-3601-2022

40. Kienast F, Ashastina A, Troeva E. Phylogeography of a west-Beringian endemic plant: an ancient seed of *Stellaria jacutica* Schischk. Detected

in permafrost deposits of the last interglacial. *Rev Palaeobot Palynol*. 2018;259:48-54. doi:10.1016/j.revpalbo.2018.09.012

41. Savvinov GN, Danilov PP, Petrov AA, Makarov VS, Boeskorov VS, Grigoriev SE. Environmental problems of the Verkhoyansk district. *Vestnik North-Eastern Fed Univ*. 2018;6(68):18-33.

42. Günther F, Grosse G, Jones BM, Schirrmeister L, Romanovsky VE, Kunitsky VV. Unprecedented permafrost thaw dynamics on a decadal time scale: Batagay mega thaw slump development, Yana uplands, Yakutia, Russia. AGU Fall Meeting, 12–16 December 2016, San Francisco. 2016.

43. Kunitsky VV, Syromyatnikov II, Schirrmeister L, et al. Ice-rich permafrost and thermal denudation in the Batagay area (Yana upland, East Siberia). *Kriosfera Zemli (Earth Cryosphere)*. 2013;17:56-58. hdl: 10013/epic.42366.d001.

44. Vadakkedath V, Zawadzki J, Przeździecki K. Multisensory satellite observations of the expansion of the Batagaika crater and succession of vegetation in its interior from 1991 to 2018. *Environ Earth Sci*. 2020;79(6):150. doi:10.1007/s12665-020-8895-7

45. Runge A, Nitze I, Grosse G. Remote sensing annual dynamics of rapid permafrost thaw disturbances with LandTrendr. *Remote Sens Environ*. 2022;268:112752. doi:10.1016/j.rse.2021.112752

46. Turetsky MR, Abbott BW, Jones MC, et al. Carbon release through abrupt permafrost thaw. *Nat Geosci*. 2020;13(2):138-143. doi:10.1038/s41561-019-0526-0

47. Murton JB. Global warming and thermokarst. In: Margesin R, ed. *Permafrost Soils*. Vol.16. Springer Berlin Heidelberg; 2009:185-203. doi:10.1007/978-3-540-69371-0_13

48. Godin E, Fortier D. Geomorphology of a thermo-erosion gully, Bylot Island, Nunavut, Canada. *Can J Earth Sci*. 2012;49(8):979-986. doi:10.1139/e2012-015

49. Kokelj SV, Jorgenson MT. Advances in thermokarst research. *Permafr Periglac Process*. 2013;24(2):108-119. doi:10.1002/ppp.1779

50. Burn CR. The thermal regime of a retrogressive thaw slump near Mayo, Yukon territory. *Can J Earth Sci*. 2000;37(7):967-981. doi:10.1139/e00-017

51. Lewkowicz AG. Nature and importance of thermokarst processes, Sand Hills moraine, Banks Island, Canada. *Geogr Ann*. 1987;69(2):321-327. doi:10.1080/04353676.1987.11880218

52. Kokelj SV, Tunnicliffe J, Lacelle D, Lantz TC, Chin KS, Fraser R. Increased precipitation drives mega-slump development and destabilization of ice-rich permafrost terrain, northwestern Canada. *Global Planet Change*. 2015;129:56-68. doi:10.1016/j.gloplacha.2015.02.008

53. Kokelj SV, Lacelle D, Lantz TC, et al. Thawing of massive ground ice in mega slumps drives increases in stream sediment and solute flux across a range of watershed scales. *J Geophys Res Earth Surface*. 2013;118(2):681-692. doi:10.1002/jgrf.20063